Check for updates

View Article Online
View Journal

Soft Matter

Accepted Manuscript

This article can be cited before page numbers have been issued, to do this please use: B. C. Druecke, A. Hooshanginejad, R. Mukherjee, P. Poureslami and S. Lee, *Soft Matter*, 2025, DOI: 10.1039/D5SM00654F.

This is an Accepted Manuscript, which has been through the Royal Society of Chemistry peer review process and has been accepted for publication.

Accepted Manuscripts are published online shortly after acceptance, before technical editing, formatting and proof reading. Using this free service, authors can make their results available to the community, in citable form, before we publish the edited article. We will replace this Accepted Manuscript with the edited and formatted Advance Article as soon as it is available.

You can find more information about Accepted Manuscripts in the Information for Authors.

Please note that technical editing may introduce minor changes to the text and/or graphics, which may alter content. The journal's standard Terms & Conditions and the Ethical guidelines still apply. In no event shall the Royal Society of Chemistry be held responsible for any errors or omissions in this Accepted Manuscript or any consequences arising from the use of any information it contains.

ROYAL SOCIETY OF CHEMISTRY

rsc.li/soft-matter-journal

View Article Online
DOI: 10.1039/D5SM00654F

Soft Matter

ARTICLE TYPE

Cite this: DOI: 00.0000/xxxxxxxxxx

Particle-laden filaments from a draining suspension†

Benjamin C. Druecke,[b‡] Alireza Hooshanginejad,[c‡] Ranit Mukherjee,[a] Parham Poureslami,[a] and Sungyon Lee*[a]

Received Date
Accepted Date

DOI: 00.0000/xxxxxxxxxx

We investigate the drainage of a suspension of non-colloidal particles from an air-filled vertical Hele-Shaw cell. When the channel gap thickness is comparable to the particle size, the suspended particles move slower than the draining fluid and cause interfacial deformations as they push against the receding oil-air interface. Distinct from the classic viscous fingering, the resultant patterns comprise thin particle-laden filaments that grow normal to an otherwise flat receding interface. When we further increase the drainage rates, we recover the classic Saffman-Taylor instability that is enhanced by the effective viscosity of the suspension. To rationalize the onset of this particle-scale instability, we derive a simple scaling law based on the force balance on a single particle entrained in a draining fluid, in reasonable agreement with our experimental data. We demonstrate that the resultant instability indeed comes from the dynamics of individual particles by reproducing it with a single particle for a narrower range of experimental parameters.

Published on 30 September 2025. Downloaded by OAKRIDGE NATIONAL LABORATORY on 10/9/2025 3:04:28 PM.

Soft Matter Accepted Manuscript

1 Introduction

Viscous fingering, one of the classic interfacial instabilities, refers to the growth of finger-like deformations of the fluid-fluid interface when a less viscous fluid displaces a more viscous fluid inside a confined channel[1–4]. Originally motivated by petroleum recovery processes[1,4–6], viscous fingering is widely studied as an "archetype" of pattern formation and growth in condensed matter physics[7], which has analogies in growth of bacterial colonies[8], dendritic growth[9], flame propagation[10], and diffusion-limited aggregation[11].

Recent studies have demonstrated that the flow configurations that lead to viscous fingering can be expanded by introducing non-colloidal particles with diameters on the order of $100\,\mu$m. For instance, injecting a particle-oil mixture into a Hele-Shaw cell gives rise to 'particle-induced viscous fingering', even in the absence of the destabilizing viscosity difference between the invading suspension and defending air[12–18]. In this flow configuration, suspended particles migrate towards the centerline between the plates due to shear-induced migration[19,20], which causes them to move faster than the mixture and accumulate on the advancing oil-air interface. The particle accumulation on the interface results in an unstable viscosity gradient inside the suspension, leading to viscous fingering.

Going beyond dynamic changes in effective viscosity, the granular nature of the suspension—the characteristics stemming from its discrete particles—can also affect viscous fingering. One manifestation of its granular nature is the frictional contact between the particles and also with the walls. There have been a number of studies investigating the injection of air into the mixture of liquid and heavy particles inside a two-dimensional (2D) cell[21–23]. Broadly termed "frictional fluid dynamics", these lab experiments reveal that the particles can settle out of the liquid and form a compaction layer on the advancing interface, imposing a frictional stress across the thin gap. Once the compaction layer forms, the finger width is set by the competition between particle friction, surface tension, and the injection pressure. Owing to its localized nature, frictional fingering can occur even without a destabilizing viscosity ratio similar to 'particle-induced viscous fingering', as recently demonstrated by Zhang et al.[24].

In both particle-induced viscous fingering and frictional fingering, the effects of particles on the fluid-fluid interface are realized on a length scale that is inherently larger than the individual particles themselves. In the case of particle-induced viscous fingering, the gradient in viscosity responsible for fingering scales with the size of the particle accumulation zone and occurs on a length scale two orders of magnitude larger than the particles[14–17,25]. For frictional fingering, the key length scale is the size of the frictional compaction layer whose growth is governed by the flux of particles to the advancing front and the stretching of the finger[23]. The compaction layer is shown to be at least an order of magnitude larger than the particle diameter[21–23]. By contrast, limited

[a] Department of Mechanical Engineering, University of Minnesota, Minneapolis, MN 55455, USA; E-mail: sungyon@umn.edu
[b] Donaldson Company, Inc., Bloomington, MN 55431, USA.
[c] SharkNinja Inc., Needham, MA 02494, USA
† Electronic Supplementary Information (ESI) available. See DOI:
‡ These authors contributed equally to this work.

DOI: 10.1039/D5SM00654F

Published on 30 September 2025. Downloaded by OAKRIDGE NATIONAL LABORATORY on 10/9/2025 3:04:28 PM.

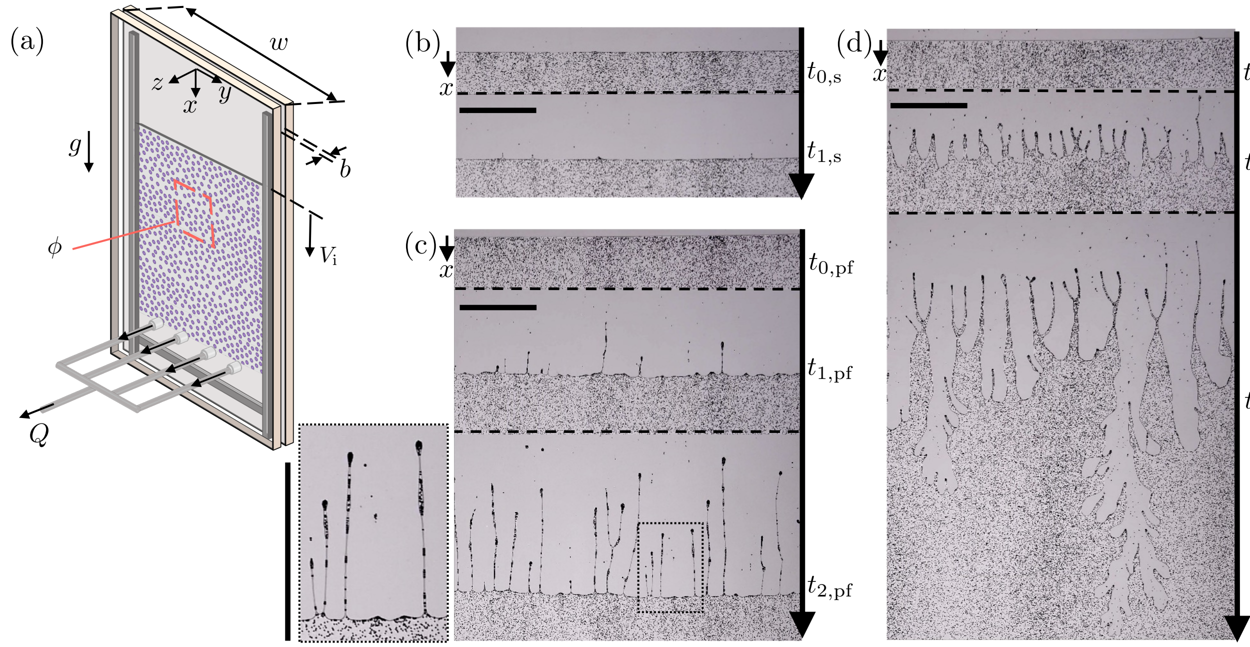

Fig. 1 (a) Schematic of the experimental set-up: The vertical Hele-Shaw cell comprises two glass plates separated by gap distance b. The suspension of particles with diameter d and uniform volume fraction ϕ is withdrawn at a constant flow rate Q, and interface velocity V_i. Suspension experiments for $\phi = 0.05$, $d = 525\,\mu$m, $b = 885\,\mu$m (i.e., $b/d \approx 1.61$): (b) snapshots from the experiments ($V_\mathrm{i} = 1.5$ mm/s) showing stable interface at $t_{0,\mathrm{s}} = 0$ s, and $t_{1,\mathrm{s}} = 30$ s; (c) snapshots showing particle-laden filaments ($V_\mathrm{i} = 3.7$ mm/s) at $t_{0,\mathrm{pf}} = 0$ s, $t_{1,\mathrm{pf}} = 20$ s, and $t_{2,\mathrm{pf}} = 60$ s; (d) snapshots showing air viscous fingers ($V_\mathrm{i} = 10.5$ mm/s) at $t_{0,\mathrm{af}} = 0$ s, $t_{1,\mathrm{af}} = 4$ s, and $t_{2,\mathrm{af}} = 12$ s. We include the zoomed-in image of particle-laden filaments in the inset of (c). All scale bars show 5 cm.

studies point to the particle-scale effects on viscous fingering, including a particle-scale "noise" to the propagating finger[26]. More recently, Luo et al.[27] uncovered the emergence of particle-scale fingers, when oil is injected into the mixture of the same oil and highly-confined particles. Here, when the smallest system dimension (i.e., channel thickness) approaches the particle size, we can observe the effects of finite particles on the invading front. This is similar to the particle-scale effects observed during the suspension droplet pinch-off, when the size of the liquid thread becomes comparable to the size of suspended particles[28–33].

In this paper, we demonstrate the particle-scale effects on pattern formation in a straightforward extension of the classic Saffman-Taylor experiments[1]. In their seminal work, Saffman and Taylor[1] discovered viscous fingering when air (fluid 1) displaces viscous liquid (fluid 2) inside a vertical Hele-Shaw cell. In the present experiments, we use the mixture of non-colloidal particles and silicone oil as the defending fluid (fluid 2), instead of pure viscous liquid as used by Saffman and Taylor[1]. Upon draining the suspension from the vertical channel, we observe the emergence of particle-laden filaments that grow normal to the stable receding oil-air interface, when the channel gap thickness is comparable to the particle diameter. In contrast to classic fingering in which air actively *invades* the draining fluid, this physical regime shows the suspension being "left behind" upon drainage in long filaments. We illustrate that these filaments are governed by the competition between destabilizing viscous effects and stabilizing effects of surface tension. As the drainage speed is increased, the particle-scale filaments and macroscopic (Saffman-Taylor) fingers appear together, forming a complex two-tiered fingering typology.

The manuscript is organized as follows. In Section 2, we introduce the experimental set-up, while the results of the suspension experiments are discussed in Section 3. In Section 4, we describe the physical mechanism behind the particle-scale thread and demonstrate its barebones physical ingredients with the discrete particle experiments. Finally, we conclude the paper with the summary and discussion of future studies in Section 5.

2 Experimental methods

As shown in the schematic in Fig. 1(a), the experimental set-up is a vertical Hele-Shaw cell comprising two rectangular glass plates (width $w = 26.7\,\mathrm{cm}$). The plates are separated by a gap thickness b whose value can be adjusted using metal shims (McMaster). We load into the cell the mixture of silicone oil (UCT, density $\rho_2 = 0.96\,\mathrm{g/cm^3}$, viscosity $\mu_2 = 0.096\,\mathrm{Pa\cdot s}$, interfacial tension $\gamma = 21\,\mathrm{mN/m}$) and non-colloidal polyethylene particles (Cospheric) with diameter d and density $\rho_p = 0.98\,\mathrm{g/cm^3}$. As over 90% of the particles fall within 5% of the mean diameter, the resultant suspension is considered fairly monodisperse.

The suspension with solid volume fraction ϕ is drained from the bottom of the cell at a constant volumetric flow rate Q, immediately after it has been loaded into the cell. This ensures that particles remain suspended in oil during the time scale of the experiments. Furthermore, the characteristic particle settling speed, given by $(\rho_\mathrm{p} - \rho_2)gd^2/(18\mu_2)$, is less than 5% of the lowest drainage speed in a typical experiment. Hence, we reasonably

Soft Matter Accepted Manuscript

View Article Online
DOI: 10.1039/D5SM00654F

Published on 30 September 2025. Downloaded by OAKRIDGE NATIONAL LABORATORY on 10/9/2025 3:04:28 PM.

consider the particles to be neutrally buoyant in this work.

Once the drainage flow is imposed, air ($\rho_1 = 1.2\,\mathrm{kg/m^3}$, $\mu_1 = 1.8\times10^{-5}\,\mathrm{Pa\cdot s}$) displaces the suspension at a mean interfacial speed V_i. We image the dynamics of the draining suspension with a Canon 60D camera (1920 × 1080 pixel images) that is placed in front of the vertical cell. We measure V_i by tracking the mean position of the interface over time and validate its value against the imposed flow rate Q. Our measurements included in Appendix A demonstrate that the experimental values of V_i deviate from $Q/(bw)$ on average by 11.1%. Accordingly, we use the experimentally measured values of V_i in subsequent analyses, instead of simply assuming $V_\mathrm{i} \approx Q/(bw)$. Finally, for a given particle-oil mixture (ϕ and d), we focus on the dynamics of the air-suspension interface upon drainage, as we systematically vary the interfacial speed V_i via changes in Q or b and the channel confinement b/d.

3 Suspension experiments

3.1 Qualitative observations

While the experimental results are general for a wide range of ϕ and d, we presently focus on the case of $\phi = 0.05$, $d = 525\,\mu\mathrm{m}$, and $b = 885\,\mu\mathrm{m}$, as we vary V_i. Our complete experimental data includes $\phi = 0.05, 0.1, 0.2, 0.3$ at $d = 525\,\mu\mathrm{m}$ (see Appendix B). Going back to the particle-free experiments where air (fluid 1) invades viscous liquid (fluid 2), Saffman and Taylor [1] identified the critical velocity, V_air^∞, for the onset of viscous (air) fingering as

$$V_\mathrm{air}^\infty = \frac{(\rho_2-\rho_1)gb^2}{12(\mu_2-\mu_1)}, \tag{1}$$

where $g = 9.8\,\mathrm{m/s^2}$ is the gravitational acceleration. Notably, V_air^∞ is set by balancing the destabilizing effects of the viscosity difference between the defending and invading fluids, $\mu_2-\mu_1$, with the stabilizing effects of the density difference, $\rho_2-\rho_1$. As the effective viscosity of the suspension increases with ϕ, the critical velocity $V_\mathrm{air} = (\rho(\phi)-\rho_1)gb^2/[12(\mu(\phi)-\mu_1)]$ for the classic fingering onset is expected to be lower than the pure oil limit, or V_air^∞.

To estimate $V_\mathrm{air}(\phi)$, we set the effective density of the suspension as $\rho(\phi) = \rho_2(1-\phi)+\rho_p\phi$ and use the following empirical expression for $\mu_(\phi)$ by Morris and Boulay [34]:

$$\frac{\mu(\phi)}{\mu_2} = 1 + 2.5\phi_\mathrm{m}\frac{\phi}{\phi_\mathrm{m}-\phi} + 0.1\frac{\phi^2}{(\phi_\mathrm{m}-\phi)^2}, \tag{2}$$

where $\phi_\mathrm{m} = 0.64$ is the maximum packing fraction. We acknowledge that Eq. (2) is intended for an unconfined suspension and may underestimate the viscosity in the monolayer limit [35]. However, it is sufficient for capturing the effects of suspended particles on air fingering in a dilute regime. Accordingly, V_air for $\phi = 0.05$ corresponds to $5.6\,\mathrm{mm/s}$, which is slightly lower than $V_\mathrm{air}^\infty \approx 6.4\,\mathrm{mm/s}$.

As demonstrated in Fig. 1(b), at $V_\mathrm{i} = 1.5\,\mathrm{mm/s}$ far below V_air, the suspension-air interface remains flat as it recedes uniformly upon drainage. This corresponds to the stable regime. When V_i is increased to $3.7\,\mathrm{mm/s}$ but still below V_air, we observe the formation and growth of thin particle-laden filaments perpendicular to the receding interface that remains relatively flat. As evident in Fig. 1(c), the width of the filaments is comparable to the particle size. In addition, the thin filaments tend to emerge from areas along the interface with higher particle concentrations (see the SI movie). Hence, their spacing depends on the particle distribution along the interface, which is not uniform. We refer to this behavior as "particle-scale fingering". Note that fingering here refers to the finger-like shape of the fluid-fluid interface, which is not limited to the classic Saffman-Taylor instability.

As V_i is further increased, the number and length of the particle-laden filaments proportionally increase. As V_i approaches V_air, the interface between the filaments starts to deform and form large-scale air fingers over time. Finally, for $V_\mathrm{i} = 10.5\,\mathrm{mm/s}$ which exceeds V_air, the particle-laden filaments and air fingers appear together, forming a complicated interfacial topology comprising both large-scale and particle-scale fingers. The evolution of this fingering behavior is clearly demonstrated in Fig. 1(d). At early times ($t_{1,\mathrm{af}}$), the particle-scale fingers first appear on the receding suspension-air interface. However, distinct from the particle fingering regime, the interface is no longer flat but is curved downward between the particle-laden filaments, which we refer to as air fingers. Over time ($t_{2,\mathrm{af}}$), the air fingers grow and even exhibit tip-splitting as observed in the classic viscous fingering experiments [4], while particle-scale fingers persist. We refer to this globally unstable regime as "air fingering".

3.2 Effects of channel confinement

The results discussed in Sec. 3.1 demonstrate the importance of the drainage speed in setting the fingering regimes at given ϕ. While increasing ϕ tends to lower the interfacial speeds at which the draining suspension becomes unstable (see Appendix B), the qualitative behavior of the receding air-suspension interface is not strongly dependent on ϕ. Hence, we fix $\phi = 0.05$ and $d = 525\,\mu\mathrm{m}$ and systematically vary V_i via the changes in Q and the gap thickness b. As varying b for given d leads to the changes in the level of channel confinement, we hereby experimentally quantify the dependence of the fingering regimes on b/d, in addition to V_i.

The phase diagram in Fig. 2(a) summarizes different behaviors of the draining suspension as a function of b/d and Ca, where $\mathrm{Ca} \equiv \mu_2 V_\mathrm{i}/\gamma$ is the capillary number. For all values of b/d, the receding suspension-air interface remains stable for $\mathrm{Ca}\to 0$ (see Fig. 1(b)); we mark the experiments that yield a stable interface with a diamond in Fig. 2(a). Then, as Ca (or V_i) is increased above $\mathrm{Ca_{air}} = \mu_2 V_\mathrm{air}/\gamma$, we observe the emergence of air fingering (circle), an example of which is shown in Fig. 1(d). Here, $\mathrm{Ca_{air}}$ follows the air fingering criterion by Saffman and Taylor [1]:

$$\mathrm{Ca_{air}} = \left(\frac{\mu_2}{\gamma}\right)\frac{(\rho(\phi)-\rho_1)gb^2}{12(\mu(\phi)-\mu_1)}, \tag{3}$$

and $\mathrm{Ca_{air}}$ is denoted with a dashed line in Fig. 2(a). This illustrates that air fingering indeed corresponds to the classic Saffman-Taylor instability, in which the presence of suspended particles primarily modifies the effective viscosity and density of the draining suspension. At the same time, the discrete nature of the particles does not play an important role in this regime.

In contrast to air fingering, Fig. 2(a) reveals that particle-scale fingering is highly dependent on the value of b/d. For $b/d < 2$, the

Soft Matter Accepted Manuscript

DOI: 10.1039/D5SM00654F

Published on 30 September 2025. Downloaded by OAKRIDGE NATIONAL LABORATORY on 10/9/2025 3:04:28 PM.

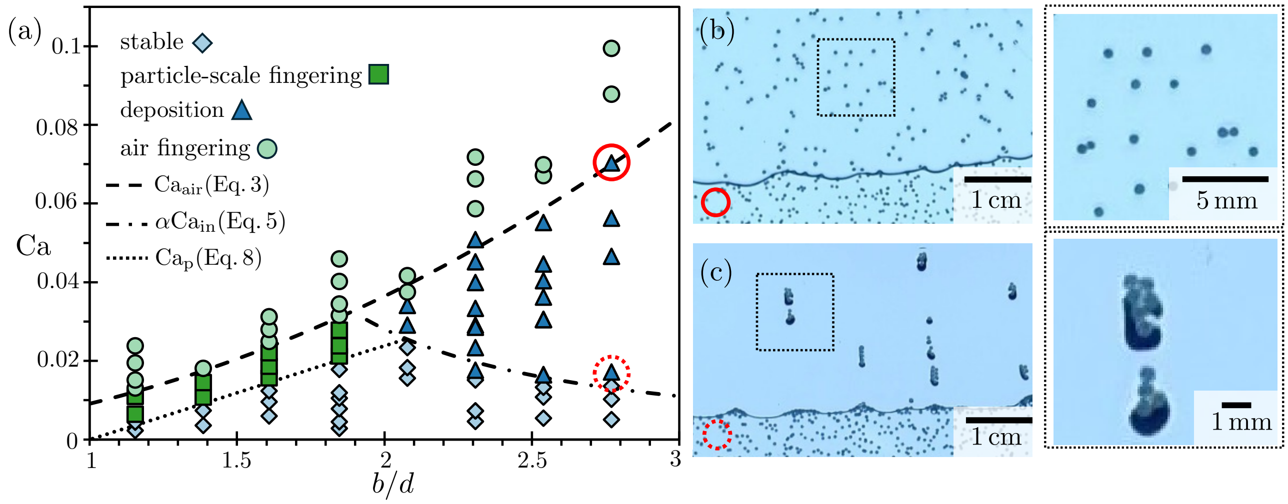

Fig. 2 (a) The phase diagram summarizing different interfacial behaviors: stable (diamond), particle-scale fingering (square), and air fingering (circle) as a function of Ca and b/d. The transition from particle-scale fingering to particle deposition (triangle) with increasing b/d is also evident in the phase map. We circle two points (Ca, b/d) in the phase diagram whose experimental images are included in (b) and (c), respectively. Experimental images showing particle deposition for $b/d = 2.77$ at two different capillary numbers: (b) $\mathrm{Ca} = 0.070$ (red solid circle); (c) $\mathrm{Ca} = 0.017$ (red dashed circle).

particle-laden filaments emerge from an otherwise flat interface (see Fig. 1(c)), as Ca is increased from the stable regime but remains below $\mathrm{Ca_{air}}$. We denote this onset of particle-scale fingering as $\mathrm{Ca_p}$, which we will rationalize in Sec. 4.1. For $b/d \geq 2$, we no longer observe particle-scale fingering; instead, the particles are deposited onto the wall as the suspension drains in this relatively low confinement regime. The particle deposition is caused by the entrainment of suspended particles into the thin film of oil that wets the wall, as frequently observed in dip coating and drainage flows[36–41]. The thickness of the wetting film h^∞ is given by[42–45]:

$$\frac{h^\infty}{b} \approx \frac{0.67\mathrm{Ca}^{2/3}}{1+3.55\mathrm{Ca}^{2/3}}. \tag{4}$$

This scaling for h^∞ was first developed by Bretherton based on lubrication approximations[42] and should hold in the thin film geometry (i.e., $h^\infty/b \ll 1$) and in the limit of zero inertia.

The particle entrainment is driven by viscous drag on the particle, while the particle-induced interfacial deformation generates a capillary force that resists entrainment[39,46]. By combining theory and experiments, Jeong and colleagues[45] demonstrated that the location of the stagnation point on the meniscus, h_s, is given by $h_s = 3h_\infty$, and particles whose diameter d is smaller than h_s tend to become entrained into the wetting film, as the viscous force overcomes the capillary force. Based on this criterion, the minimum capillary number above which individual particles are likely entrained corresponds to

$$\mathrm{Ca_{in}} \approx \left[4.02\left(\frac{b}{d}\right) - 3.55\right]^{(-3/2)}. \tag{5}$$

The onset of particle deposition predicted by $\mathrm{Ca_{in}}$ is consistently higher than our experimental data.

This discrepancy between theory and experiments can be explained by noting that $\mathrm{Ca_{in}}$ is set for individual particles, not suspensions. When multiple particles are present in the draining oil, suspended particles tend to form clusters and get entrained into the thin film at a fraction of $\mathrm{Ca_{in}}$, or $\alpha\mathrm{Ca_{in}}$, where $\alpha < 1$. This rather counterintuitive result was first explained by Colosqui et al.[39] whose simulations show the particles assembling into a packed monolayer in dip coating flows. The resultant monolayer experiences enhanced viscous drag, while the local interfacial curvature and the resultant capillary force are reduced. As a result, the particle cluster in a monolayer is entrained into a wetting film at a capillary number that is lower than $\mathrm{Ca_{in}}$. Then, the onset of particle deposition in our experiments is well described by setting $\alpha \approx 0.3$, as $\alpha\mathrm{Ca_{in}}$ is denoted with a dash-dotted line in Fig. 2(a). This empirical value of α matches the findings of Sauret and colleagues[46] who experimentally measured Ca of cluster entrainment upon dip coating of suspensions. Specifically, at $\phi = 0.05$, they found that Ca of cluster entrainment is approximately 30% of $\mathrm{Ca_{in}}$, or $\alpha \approx 0.3$, while α increases to approximately 0.5 at $\phi = 0.02$.

To illustrate the changes in particle deposition with the drainage speed, we include two experimental images at $b/d = 2.77$, for two different values of Ca. At $\mathrm{Ca} = 0.070$ far above $\mathrm{Ca_{in}} \approx 0.027$, individual particles are deposited onto the glass wall, as evident in the image in Fig. 2(b). By contrast, the experimental image in Fig. 2(c) reveals particle clusters that are left behind as the air-oil interface recedes at $\mathrm{Ca} = 0.017$, slightly above $\alpha\mathrm{Ca_{in}} \approx 0.014$. This confirms that the presence of neighboring particles indeed enables the particle entrainment into the wetting film far below $\mathrm{Ca_{in}}$ via cluster formation.

Going back to the fingering regimes in Fig. 2, air fingering appears mostly unaffected by particle deposition as the two regimes are observed together. This is also evidenced by the fact that the onset of air fingering is reasonably predicted by $\mathrm{Ca_{air}}$ in Eq. (3) for the entire b/d range. Similarly, particle-laden filament and particle deposition regimes are expected to overlap when $b/d > 1.90$ and $\mathrm{Ca} < \mathrm{Ca_{air}}$, as $\alpha\mathrm{Ca_{in}}$ intersects $\mathrm{Ca_{air}}$ at $b/d \approx 1.90$. However,

Soft Matter Accepted Manuscript

View Article Online
DOI: 10.1039/D5SM00654F

Published on 30 September 2025. Downloaded by OAKRIDGE NATIONAL LABORATORY on 10/9/2025 3:04:28 PM.

Soft Matter Accepted Manuscript

the formation of particle-laden filaments appears to be "overtaken" by particle deposition, which hints at the close connection between the two regimes. In the next section, we describe the physical mechanism behind particle-scale fingering as well as its similarities and differences to particle deposition.

4 Discrete particle experiments

4.1 Physical mechanism of particle-scale fingering

The experimental observations in Fig. 2 suggest that the following two physical conditions are necessary to induce particle-scale fingering: (i) high channel confinement (i.e., small b/d) and (ii) sufficiently large Ca that remains below $\mathrm{Ca}_{\mathrm{air}}$. First, the high channel confinement ensures that the particles may move slower than the average drainage velocity V_{i} even at the channel centerline, as numerically simulated for a single particle inside a pressure-driven channel flow[47]. The experiments of highly confined particles inside a 2D channel[27,48] also confirm a lag in the particle speed V_{p} relative to the background flow, leading to dipolar interactions between particles[49]. Since $V_{\mathrm{p}} < V_{\mathrm{i}}$, particles tend to collect near the receding oil-air interface. At the same time, small b/d ensures that the particles do not become entrained into the wetting film unless Ca is increased far above $\mathrm{Ca}_{\mathrm{air}}$ for $b/d < 1.90$.

To rationalize the minimum drainage speed, or the critical capillary number Ca_{p}, needed to induce particle-scale fingering, we consider a single particle on the receding oil-air interface for simplicity. This follows from our conjecture that the presence of neighboring particles may enhance but is not required for the particle-scale liquid thread to form. To demonstrate this, we conduct experiments with a single particle with $d \approx 1\,\mathrm{mm}$ that is drained downward inside a vertical Hele-Shaw cell with $b = 1035\,\mu\mathrm{m}$ (i.e., $b/d \approx 1.04$). The drainage speed at the onset of air fingering corresponds to $V_{\mathrm{air}}^{\infty} \approx 8.7\,\mathrm{mm/s}$ via Eq. (1). At $V_{\mathrm{i}} = 6\,\mathrm{mm/s} < V_{\mathrm{air}}^{\infty}$, the particle in Fig. 3(a) first approaches the receding interface, confirming that a highly confined particle may move slower than the background flow. We further quantify this by plotting the particle speed V_{p} together with V_{i} as a function of time in Fig. 7(a), which shows that $V_{\mathrm{p}} < V_{\mathrm{i}}$ initially. Once the particle meets the receding interface, the interface resists deformation due to the effects of surface tension and causes the particle to move down at V_{i}, corresponding to the stable regime. Accordingly, V_{p} coincides with V_{i} at this time in Fig. 7(a).

When V_{i} is increased to $10\,\mathrm{mm/s}$ above $V_{\mathrm{air}}^{\infty}$, the particle on the interface behaves as a disturbance that initiates the Saffman-Taylor fingering, as shown in Fig. 3(c). Similar to the stable regime, V_{p} is shown to catch up to V_{i} after it reaches the interface (see Fig. 7(c)). Finally, at $V_{\mathrm{i}} = 7\,\mathrm{mm/s} < V_{\mathrm{air}}^{\infty}$ in Fig. 3(b), the particle upon reaching the interface continues to move slower than V_{i} and generates a particle-scale fingering. We emphasize again that fingering here refers to the finger-like deformation and stretching of the interface, not limited to the Saffman-Taylor instability. The particle slowdown relative to the interface is made clear in the plot of V_{p} and V_{i} in Fig. 7(b), which shows V_{p} fluctuating in value consistently below V_{i}.

The transition from the stable regime to particle-induced fingering in Fig. 3(b)-(c) can be understood by considering the forces acting on the particle when it reaches the interface. We set $V_{\mathrm{p}} = V_{\mathrm{i}}$ and derive the scaling for the minimum drainage speed for particle-induced fingering, by making a number of significant assumptions we outline here. First, we assume the flow around the particle can be modeled using Darcy's law (i.e., $\partial p/\partial x = \rho_2 g - 12\mu_2 V/b^2$) and neglect the effects of the fluid-fluid interface on the flow. Second, we consider a highly confined particle (i.e., $b/d \to 1$) that is positioned at the centerline between the two vertical walls. In this limit, we break up the forces on the particle into the pressure drag from the Darcy flow and the viscous shear on the particle due to the proximity to the no-slip walls. Given these major simplifications, the objective of our model is to qualitatively capture the dependence of Ca_{p} on b/d with the minimum physical ingredients, instead of making a quantitative prediction.

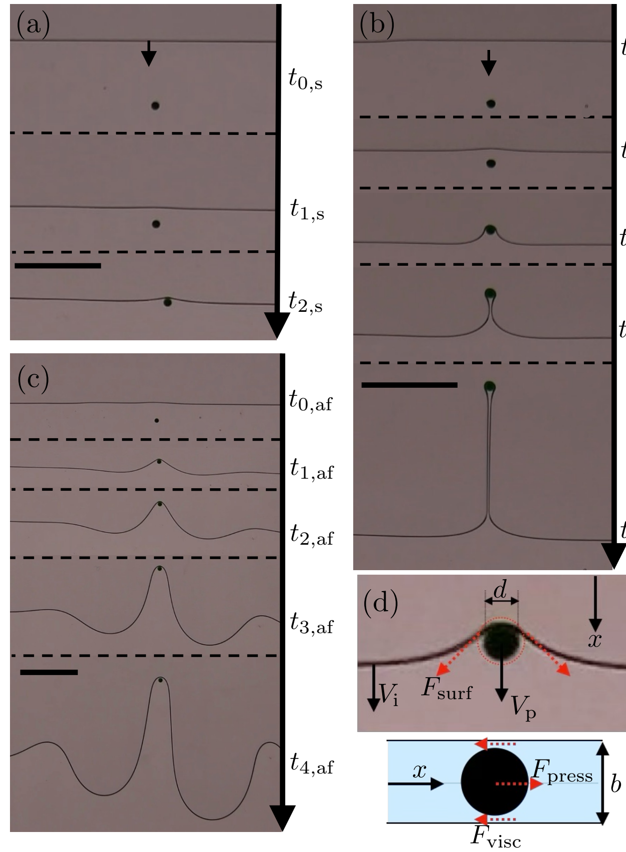

Fig. 3 (a) Snapshots from the single-particle experiments showing stable interface for $b/d \approx 1.04$ (i.e., $d = 1000\,\mu\mathrm{m}$, $b = 1035\,\mu\mathrm{m}$) and $V_{\mathrm{i}} = 6$ mm/s at $t_{0,\mathrm{s}} = 0$ s, $t_{1,\mathrm{s}} = 6$ s, and $t_{2,\mathrm{s}} = 10$ s. (b) Snapshots from the single-particle experiments showing particle-scale fingering for $b/d \approx 1.04$ and $V_{\mathrm{i}} = 7$ mm/s at $t_{0,\mathrm{pf}} = 0$ s, $t_{1,\mathrm{pf}} = 3$ s, $t_{2,\mathrm{pf}} = 4$, $t_{3,\mathrm{pf}} = 5$ s, and $t_{4,\mathrm{pf}} = 9$ s. (c) Snapshots from the single-particle experiments showing air fingering for $d = 1000\,\mu\mathrm{m}$, $b = 1035\,\mu\mathrm{m}$, and $V_{\mathrm{i}} = 10$ mm/s at $t_{0,\mathrm{af}} = 0$ s, $t_{1,\mathrm{af}} = 6$ s, $t_{2,\mathrm{af}} = 9$, $t_{3,\mathrm{af}} = 12$ s, and $t_{4,\mathrm{af}} = 15$ s. All scale bars show 1 cm. (d) The schematics of the forces acting on a single particle on the interface.

As illustrated in the schematic of Fig. 3(d), the particle in contact with the draining interface is bound to deform the interface. This generates the surface tension force, $F_{\mathrm{surf}} \propto \gamma d$, that pushes the particle in the x-direction. At the same time, the particle ex-

View Article Online
DOI: 10.1039/D5SM00654F
Published on 30 September 2025. Downloaded by OAKRIDGE NATIONAL LABORATORY on 10/9/2025 3:04:28 PM.
Soft Matter Accepted Manuscript

periences the pressure drag from the surrounding flow:

$$F_{\mathrm{press}} = \frac{\pi}{6} d^3 \left[12\mu_2 \frac{V_{\mathrm{i}}}{b^2} - \rho_2 g \right], \tag{6}$$

which we estimate based on Darcy's law. Since the particle density ρ_p closely matches ρ_2, the pressure drag contribution from the body force is canceled out by the particle weight, $W = (\pi/6)\rho_p g d^3$. Due to the channel confinement, there is an additional viscous force coming from the thin lubricating layer between the particle and the walls, $F_{\mathrm{visc}} \propto 2\mu_2 \pi d^2 V_{\mathrm{i}}/(b-d)$, as illustrated in Fig. 3(d). While F_{press} and F_{surf} push the particle down in the x-direction, F_{visc} tends to slow down the particle and push it towards the interface, hence, inducing particle-scale fingering.

Putting all the forces together, we arrive at the following force balance in the x-direction:

$$2\pi d^3 \mu_2 \frac{V_{\mathrm{i}}}{b^2} + C\gamma d = \beta \pi d^2 \mu_2 \frac{V_{\mathrm{i}}}{(b-d)/2}, \tag{7}$$

where C and β are the unknown prefactors. We set $C = 1$ for simplicity and re-organize Eq. (7) to derive the following expression for the critical capillary number for particle fingering, or $\mathrm{Ca_p}$:

$$\mathrm{Ca_p} \propto \frac{b/d}{2\pi} \left[\frac{\beta}{1-(d/b)} - \left(\frac{d}{b} \right) \right]^{-1}. \tag{8}$$

We plot the resultant $\mathrm{Ca_p}$ as a function of b/d in Fig. 2(a), which reasonably describes the boundary between the stable and particle fingering regimes when we set $\beta \approx 6.9$. Here, we emphasize again that the quantitative match between the model and the experiments is unimportant, especially given that the value of β was fitted to achieve this. The primary goal is to show that Eq. (8) captures the increasing trend in $\mathrm{Ca_p}$ with b/d, despite the number of significant simplifications in the model. In addition, since the derivation of Eq. (8) is strictly valid for $b/d \to 1$, we expand $\mathrm{Ca_p}$ in the limit of $\varepsilon \to 0$, where $\varepsilon \equiv (b/d) - 1$:

$$\mathrm{Ca_p} \approx \frac{1}{2\pi} \left[\frac{\varepsilon}{\beta} + \frac{\varepsilon^2}{\beta^2} + O(\varepsilon^3) \right]. \tag{9}$$

Eq. (9) predicts that, to the leading order, $\mathrm{Ca_p}$ increases linearly with b/d and vanishes at $b/d = 1$, which matches the experimental data in Fig. 2(a).

Going back to the physical mechanism, particle-scale fingering is caused by the enhanced viscous stresses on the particle and is resisted by the combination of surface tension and the pressure drag coming from the surrounding flow. This has a clear parallel to the physical mechanism of particle deposition, where viscous drag opposes the surface tension force[39,46]. However, particle-scale fingering does not require the particle to be entrained into a thin wetting film. The only requisite condition for a particle-scale finger to form is for the particle to move slower than the draining interface, which holds for particles whose size is comparable to the gap thickness so that $F_{\mathrm{visc}} > F_{\mathrm{press}} + W$. When such large particles encounter the receding interface, they cause the visible *in-plane interfacial deformation*, that we refer to as a "particle-scale" instability.

The distinction between particle-scale fingering and particle deposition becomes more clear when we consider how the onset of the two regimes varies with b/d. In contrast to $\mathrm{Ca_p}$ that increases with b/d, the minimum capillary number at which particle deposition is observed decreases with b/d. As discussed in Sec. 3.2, for a particle (or a particle cluster) to be entrained into the thin film, its size must be comparable to the thickness of the wetting film h^{∞} that increases with b and the capillary number. Hence, a particle or a particle cluster that is entrained into the thin film is likely not large enough to generate an in-plane deformation of the interface. This renders the two regimes mostly mutually exclusive, as evident in Fig. 2(a). However, there are exceptions to this general trend, which we discuss in Sec. 4.2

4.2 Effects of neighboring particles

While the physical mechanism of particle-scale fingering can be rationalized with a single particle, the presence of multiple particles in the draining oil affects the fingering onset. When a mixture of non-colloidal particles and oil drains from a vertical cell, particles tend to form clusters near the receding oil-air interface, which enhances the effective viscous force F_{visc} and is more likely to yield particle-scale fingering. In some cases, particle clusters that deform the receding interface can also come into contact with the wall and become stationary. Such clusters become deposited onto the wall and also form particle-laden filaments that eventually pinch off. This corresponds to the rare cases where particle-scale fingering and particle deposition appear together.

We can qualitatively observe the evidence of cluster formation in the drainage experiments (i.e., $d = 1000\,\mu$m and $b = 1035\,\mu$m), where we systematically increase the number of particles n from one to four (by one particle increment) and then up to 30, as shown in Fig. 4(a). Excepting the case with only one particle, multiple particles are shown to be part of a growing finger, indicating that neighboring particles form a cluster and collectively cause the interfacial deformation.

Analogous to particle deposition, the cluster formation tends to expand the physical parameter space (i.e., lower V_{i} and larger b/d) under which particle-scale fingering is observed. We again demonstrate this by conducting drainage experiments with an increasing number of particles n and observing the dynamics of the receding interface for varying V_{i}. Since we are working with a very small number of particles, the resultant behaviors are sensitive to each particle's initial position inside the gap that cannot be precisely controlled. In fact, our simple scaling law for $\mathrm{Ca_p}$ in Eq. (8) assumes the particle travels at the centerline between the two walls. A particle that is off-center would rotate due to flow asymmetry, which changes the force and torque balance. Hence, we do not expect Eq. (8) to be able predict the onset of particle fingering even for a single particle whose position inside the gap is not known and cannot be controlled. This renders obtaining consistent experimental results difficult. Hence, at given n and V_{i}, we repeat the experiments at least five times and plot the probability p of different fingering regimes that are observed, instead of aiming to pin down the onset of particle-scale fingering.

The plots in Fig. 4(b)-(f) indeed show that the overall occurrence of particle-scale fingering increases when more particles are

View Article Online
DOI: 10.1039/D5SM00654F

Published on 30 September 2025. Downloaded by OAKRIDGE NATIONAL LABORATORY on 10/9/2025 3:04:28 PM.

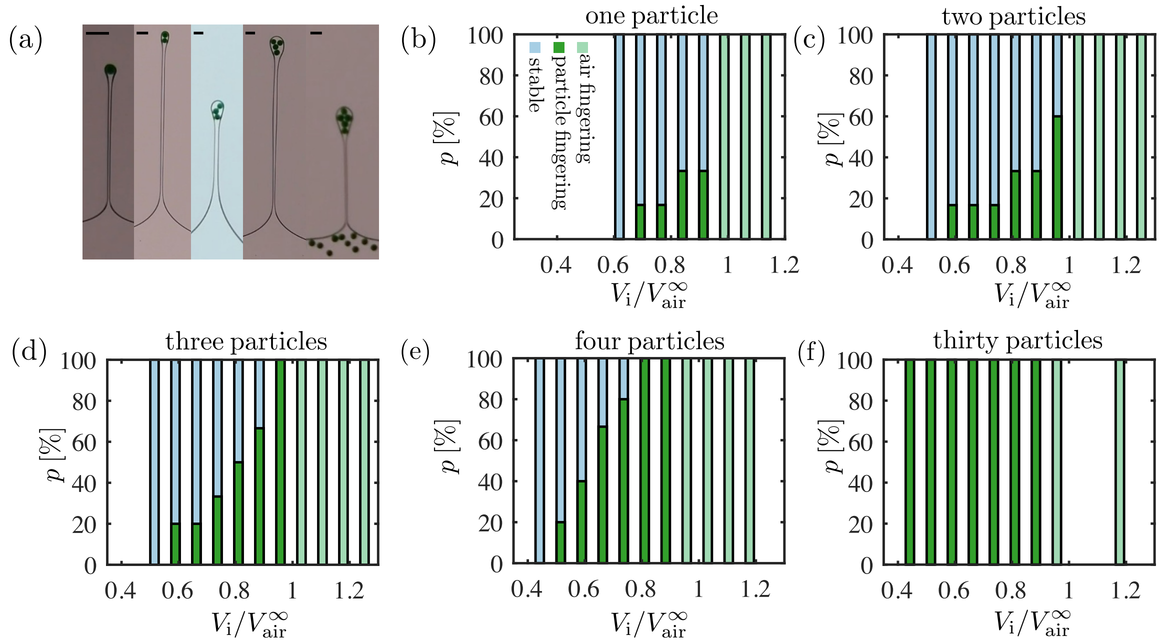

Fig. 4 (a) Snapshots of discrete particles experiments showing particle-scale fingering for $n = 1$, 2, 3, 4, and 30 particles with $d = 1000\,\mu$m and $b = 1035\,\mu$m, or $b/d \approx 1.04$. The scale bars show 2 mm. (b) Single-particle, (c) two-particles, (d) three-particles, (e) four-particles, and (f) thirty-particles probability plots for $b/d \approx 1.04$, as a function of V_i/V_{cr}.

added to the draining oil. Furthermore, particle fingering is observed at increasingly lower V_i with increasing n. For instance, for a single particle, the minimum drainage speed at which particle fingering is observed corresponds to $V_i/V_{air}^{\infty} \approx 0.69$, where $V_{air}^{\infty} \approx 8.7\,$mm/s. With $n = 4$, the minimum speed decreases to $V_i/V_{air}^{\infty} \approx 0.52$, while we observe particle fingering 100% of the time for V_i/V_{air}^{∞} as low as 0.44 at $n = 30$. In addition, the probability plots reveal that air fingering occurs consistently for $V_i > V_{air}^{\infty}$, again validating that air fingering is insensitive to the granular nature of the suspended particles. When n is increased to four and then to 30, air fingering is observed at $V_i \approx 8.37\,$mm/s, which is slightly below $V_{air}^{\infty} \approx 8.74\,$mm/s. This indicates that as little as four particles may locally increase the effective viscosity of the draining mixture, which in turn lowers the minimum speed for air fingering.

Finally, it is important to point out that suspension experiments yield mostly consistent results, despite the probabilistic nature of individual particle experiments. As previously described, for a single particle, its position inside the gap is important in determining the critical interfacial speed to generate a particle-scale thread. When many particles are present in the draining liquid, they form a cluster near the interface, which renders their precise position inside the gap unimportant. This is why the onset of instability is no longer probabilistic for a suspension, which is already evident even with the 30-particle experiments in Fig. 4(f). Furthermore, we hypothesize that the characteristic size of the particle cluster likely increases with the particle concentration ϕ, which in turn lowers the critical interfacial speed for the particle-scale finger formation. This is consistent with the result of our additional suspension experiments in Fig. 6 that shows a decrease in Ca_p with increasing ϕ.

5 Conclusions

In this paper, we experimentally demonstrate the emergence of an interfacial instability that depends on the granular nature of the suspension, when the particle and oil mixture drains from a vertical Hele-Shaw cell. For all channel confinement b/d, the receding suspension-air interface remains stable at low interfacial speed V_i, while classic air fingering is observed at high V_i, or $V_i > V_{air}$, where V_{air} follows the criterion set by Saffman and Taylor[1]. Then, only in a highly confined regime (i.e., $1 < b/d < 2$), we observe narrow, particle-rich interfacial fingers that grow perpendicularly to a relatively flat receding interface at intermediate V_i. We experimentally quantify this fingering regime by constructing a phase diagram as a function of the capillary number Ca and b/d. The resultant phase diagram confirms the emergence of particle-scale fingering in a highly confined regime, which transitions to the entrainment of particles into the wetting film at larger b/d, also observed in dip coating and drainage flows[45,46].

We hypothesize that particle-scale fingering stems from the enhanced viscous forces on a draining particle due to the channel confinement. Based on the force balance on a single particle, we derive a scaling law for the critical capillary number for particle-scale fingering Ca_p, in good qualitative agreement with the experimental data. Furthermore, as the physical mechanism described should be realizable with a single particle, we conduct a series of drainage experiments with single particles. These additional experiments reveal that particle-scale fingering can indeed occur with just one particle but is greatly aided by the presence of neighboring particles that expand the parameter regime (i.e., lower V_i) in which particle-scale fingering is observed.

Along with the recent work by Luo et al.[27], our experiments demonstrate particle-scale morphologies in the displace-

Soft Matter Accepted Manuscript

Published on 30 September 2025. Downloaded by OAKRIDGE NATIONAL LABORATORY on 10/9/2025 3:04:28 PM.

ment flows involving non-colloidal particles, as the channel gap approaches the size of the suspended particles or particle clusters. The emergence of length scales that are comparable to the finite particle size distinguishes the current system from the classic Saffman-Taylor instability with pure fluids. At the same time, particle-scale fingering is driven by viscous effects and is distinct from frictional fingering that requires the frictional contact between the particles and the walls[21–23,26].

Future work involves quantifying and controlling particle-laden filaments for wider experimental parameters, including uncovering what sets the length of the particle-laden filaments. In addition, recent computational studies[35,50,51] have revealed strong effects of the channel confinement on the suspension rheology in a highly concentrated regime. For instance, Fornari et al.[51] found that the viscosity of a dense suspension is reduced when the gap size is about twice the particle diameter. This is attributed to the particles self-organizing into two "sliding" layers[51]. Hence, it would be of great interest to revisit our current experiments with a much higher concentration (i.e., $\phi > 0.3$) to see how the confinement-induced changes in the suspension rheology affects the fingering regimes. Finally, our preliminary experiments with a bidisperse suspension reveal that small particles are entrained into the thin film, while larger particles form particle-laden fingers. Hence, we will further explore this new particle segregation mechanism and pattern formation driven by channel confinement as future work.

Author Contributions

S.L. supervised the research and wrote the manuscript. B.D., A.H., and S.L. designed the research questions. B.D. and A.H. designed and performed the experiments, processed the data, and helped construct the figures. R.M. and P.P. performed additional experiments and helped complete the manuscript.

Data Availability

The data supporting this article have been included as part of the ESI.†

Conflicts of interest

The authors declare no conflicts of interest.

Acknowledgements

We would like to acknowledge Ms. Jenna Brown for taking preliminary experimental data. This work was partly funded by National Science Foundation (CBET-2032354, DMR-2003706, EAR-2100493).

Appendices

A. Validating the syringe pump rate

Fig. 5 shows the result of calibrating the syringe pump withdrawal rate Q against the measured interface velocity V_i. Our measurements indicate that the experimental interface speed obtained from image analysis is slightly lower than the theoretical value given by Q/bw. Quantitatively, the mean and standard deviation of the relative error between the theoretical and experimental interface speeds are 11.1% and 11.0%, respectively.

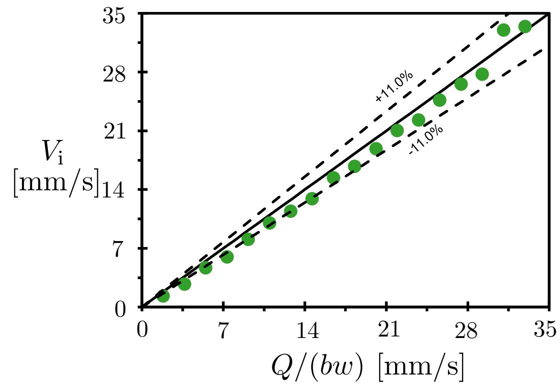

Fig. 5 Experimentally measured interface speed compared with the theoretical prediction (Q/bw). The solid line represents the line of slope 1, and the dashed lines denote the standard deviation of the relative error, within which 72% of the data lie.

B. Fingering regimes for varying ϕ

We plot the fingering regimes for varying ϕ and the capillary number Ca, while we fix the mean particle diameter (i.e., $d = 525\,\mu$m) and the channel confinement $b/d = 1.21$. The results in Fig. 6 show that the onset of air fingering decreases with ϕ, which qualitatively matches the decrease in theoretical $\mathrm{Ca_{air}}$ due to the increase in the effective viscosity. The plot also shows that the critical capillary number for particle fingering decreases with ϕ. This result is also consistent with the fact that the presence of neighboring particles causes particle-scale fingering to occur at lower V_i, as the particles cluster together.

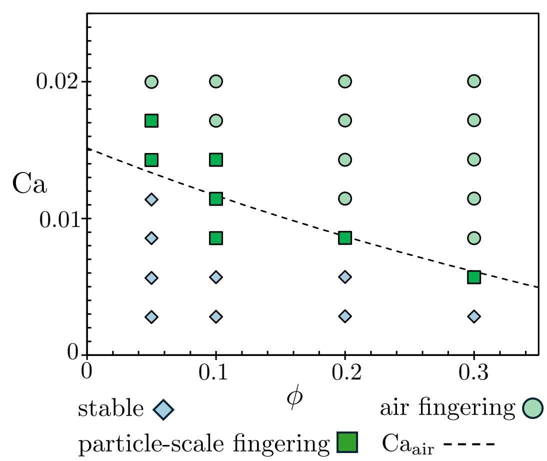

Fig. 6 A regime map of different interfacial dynamics as a function of the capillary number Ca and the particle volume fraction ϕ: stable (diamond), particle-scale fingering (square), and air fingering (circle). All the experiments are performed with $d = 525\,\mu$m and $b/d = 1.21$.

C Particle speed versus interfacial speed

We extract the speeds of the particle (V_p) and of the draining interface (V_i) for the single particle experiments shown in Fig 3. The plots point to some interesting features of the coupled particle-interface motion. For both stable and air fingering regimes, the particle initially moves slower than the interface (i.e., $V_p < V_i$)

Soft Matter Accepted Manuscript

Published on 30 September 2025. Downloaded by OAKRIDGE NATIONAL LABORATORY on 10/9/2025 3:04:28 PM.

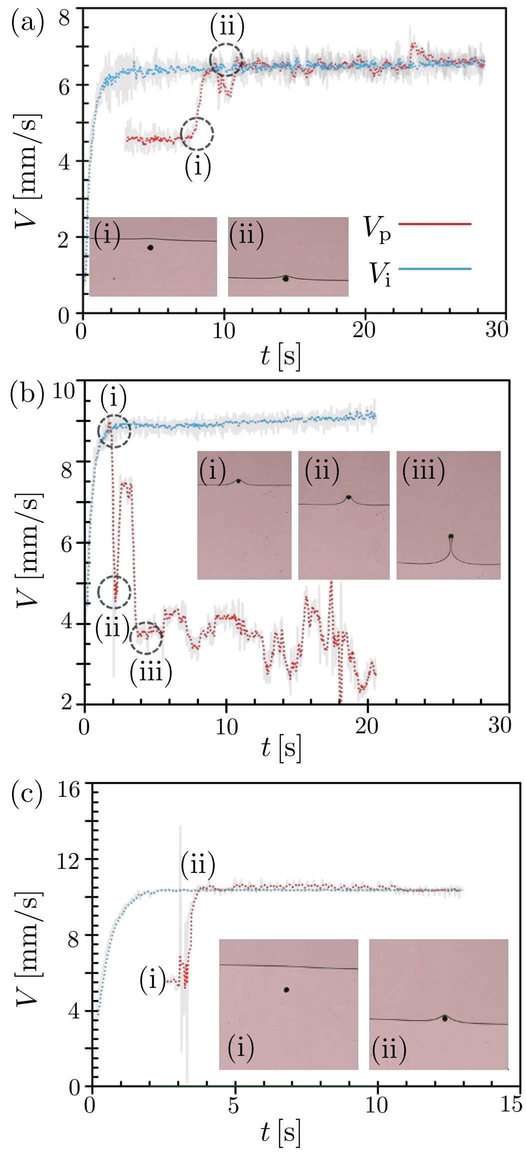

Fig. 7 Comparison of individual particle speed (V_p) to the interface speed (V_i) in stable, particle fingering, and air fingering regimes, respectively. (a) In the stable regime ($V_i =, 6$ mm/s), V_p initially lags behind V_i but quickly catches up to V_i, as the interface reaches the particle. The inset images (i and ii) show the exact frames where the speed transition happens. (b) In the particle fingering regime ($V_i =, 8$ mm/s), the particle slows down as the interface bends around it (inset image (ii)). Finally, the interface wraps the particle as it moves away (inset (iii)), dragging it at an average speed of 3.6 mm/s. (c) In the air fingering regime ($V_i =, 10$ mm/s), the particle begins to move at the interface speed once it comes into contact with the interface. All the experiments are done within a Hele-Shaw cell of confinement ratio, $b/d = 1.035$. The particle size in all the videos is $d = 1$ mm, which also serves as the scale for the images.

when the interface is more than one particle diameter away. However, as the interface moves closer to the particle, the particle slowly speeds up and moves with the interface, such that $V_p = V_i$. Only in the particle-scale fingering regime, V_p remains consistently lower than V_i even after it comes into contact with the interface. Furthermore, V_p is shown to fluctuate widely (all below V_i), as the interface engulfs the particle and forms a long liquid thread.

Notes and references

1 P. G. Saffman and G. I. Taylor, *P. Roy. Soc. Lond. A Mat.*, 1958, **245**, 312–329.
2 P. G. Saffman, *Journal of Fluid Mechanics*, 1986, **173**, 73–94.
3 L. Paterson, *J. Fluid Mech.*, 1981, **113**, 513–529.
4 G. M. Homsy, *Annu. Rev. Fluid Mech.*, 1987, **19**, 271–311.
5 S. Hill and F. I. P, *Chemical Engineering Science*, 1952, **1**, 247–253.
6 R. L. Chuoke, P. van Meurs and C. van der Poel, *The Instability of Slow, Immiscible, Viscous Liquid-Liquid Displacements in Permeable Media*.
7 Y. Couder, *Perspectives in Fluid Dynamics*, Cambridge University Press, 2000.
8 E. Ben-Jacob, H. Shmueli, O. Shochet and A. Tenenbaum, *Physica A: Statistical Mechanics and its Applications*, 1992, **187**, 378 – 424.
9 A. K. McAllister, *Cereb. Cortex*, 2000, **10**, 963 – 973.
10 C. Clanet and G. Searby, *Phys. Rev. Lett.*, 1998, **80**, 3867–3870.
11 J. Mathiesen, I. Procaccia, H. L. Swinney and M. Thrasher, *EPL (Europhysics Letters)*, 2006, **76**, 257.
12 H. Tang, W. Grivas, D. Homentcovschi, J. Geer and T. Singler, *Phys. Rev. Lett.*, 2000, **85**, 2112–2115.
13 A. Ramachandran and D. T. Leighton, *J. Rheol.*, 2010, **54**, 563 – 589.
14 F. Xu, J. Kim and S. Lee, *J. Non-Newton. Fluid*, 2016, **238**, 92 – 99.
15 J. Kim, F. Xu and S. Lee, *Phys. Rev. Lett.*, 2017, **118**, 074501.
16 R. Luo, Y. Chen and S. Lee, *Phys. Rev. Fluids*, 2018, **3**, 110502.
17 F. Xu and S. Lee, *Journal of Fluid Mechanics*, 2019, **860**, 487–509.
18 A. Hooshanginejad, B. C. Druecke and S. Lee, *Journal of Fluid Mechanics*, 2019, **869**, R2.
19 D. Leighton and A. Acrivos, *J. Fluid Mech.*, 1987, **181**, 415–439.
20 D. Leighton and A. Acrivos, *J. Fluid Mech.*, 1987, **177**, 109–131.
21 B. Sandnes, E. G. Flekkoy, H. A. Knudsen, K. J. Maloy and H. See, *Nat. Commun.*, 2011, **2**, 288.
22 J. A. Eriksen, R. Toussaint, K. J. Måløy, E. Flekkøy, O. Galland and B. Sandnes, *Phys. Rev. Fluids*, 2018, **3**, 013801.
23 E. G. Flekkøy, B. Sandnes and K. J. Måløy, *Phys. Rev. Fluids*, 2023, **8**, 114302.
24 D. Zhang, J. M. Campbell, J. A. Eriksen, E. G. Flekkøy, K. J. Måløy, C. W. MacMinn and B. Sandnes, *Nature Communications*, 2023, **14**, 3044.
25 Y. Chen, R. Luo, L. Wang and S. Lee, *Journal of Fluid Mechanics*, 2021, **925**, A10.
26 C. Chevalier, A. Lindner and E. Clément, *Phys. Rev. Lett.*, 2007, **99**, 174501.
27 R. Luo, M. Marshall, Z. He, L. Wang and S. Lee, *Journal of*

Soft Matter Accepted Manuscript

View Article Online
DOI: 10.1039/D5SM00654F

Fluid Mechanics, 2025, **1011**, A48.
28 R. J. Furbank and J. F. Morris, *Phys. Fluids*, 2004, **16**, 1777–1790.
29 R. J. Furbank and J. F. Morris, *Int. J. Multiphas. Flow*, 2007, **33**, 448 – 468.
30 C. Bonnoit, T. Bertrand, E. Clément and A. Lindner, *Phys. Fluids*, 2012, **24**, 043301.
31 T. Bertrand, C. Bonnoit, E. Clément and A. Lindner, *Granul. Matter*, 2012, **14**, 169–174.
32 M. Z. Miskin and H. M. Jaeger, *P. Natl. Acad. Sci. USA*, 2012, **109**, 4389–4394.
33 M. S. van Deen, T. Bertrand, N. Vu, D. Quéré, E. Clément and A. Lindner, *Rheol. Acta*, 2013, **52**, 403–412.
34 J. F. Morris and F. Boulay, *J. Rheol.*, 1999, **43**, 1213–1237.
35 Y. Davit and P. Peyla, *Europhysics Letters*, 2008, **83**, 64001.
36 M. Ghosh, F. Fan and K. J. Stebe, *Langmuir*, 2007, **23**, 2180–2183.
37 S. Watanabe, K. Inukai, S. Mizuta and M. T. Miyahara, *Langmuir*, 2009, **25**, 7287–7295.
38 J. C. T. Kao and A. E. Hosoi, *Physics of Fluids*, 2012, **24**, 041701.
39 C. E. Colosqui, J. F. Morris and H. A. Stone, *Phys. Rev. Lett.*, 2013, **110**, 188302.
40 Y. Chen, F. Malambri and S. Lee, *Phys. Rev. Fluids*, 2018, **3**, 094001.
41 A. Gans, E. Dressaire, B. Colnet, G. Saingier, M. Z. Bazant and A. Sauret, *Soft Matter*, 2019, **15**, 252–261.
42 F. P. Bretherton, *Journal of Fluid Mechanics*, 1961, **10**, 166–188.
43 C. W. Park and G. M. Homsy, *Journal of Fluid Mechanics*, 1984, **139**, 291–308.
44 P. Aussillous and D. Quéré, *Physics of Fluids*, 2000, **12**, 2367–2371.
45 D.-H. Jeong, A. Kvasnickova, J.-B. Boutin, D. Cébron and A. Sauret, *Phys. Rev. Fluids*, 2020, **5**, 114004.
46 A. Sauret, A. Gans, B. Colnet, G. Saingier, M. Z. Bazant and E. Dressaire, *Phys. Rev. Fluids*, 2019, **4**, 054303.
47 M. E. Staben, A. Z. Zinchenko and R. H. Davis, *Physics of Fluids*, 2003, **15**, 1711–1733.
48 T. Beatus, R. H. Bar-Ziv and T. Tlusty, *Physics Reports*, 2012, **516**, 103–145.
49 N. Desreumaux, J. Caussin, R. Jeanneret, E. Lauga and D. Bartolo, *Physical Review Letters*, 2013, **111**, 118301.
50 V. Doyeux, S. Priem, L. Jibuti, A. Farutin, M. Ismail and P. Peyla, *Phys. Rev. Fluids*, 2016, **1**, 043301.
51 W. Fornari, L. Brandt, P. Chaudhuri, C. U. Lopez, D. Mitra and F. Picano, *Phys. Rev. Lett.*, 2016, **116**, 018301.

Published on 30 September 2025. Downloaded by OAKRIDGE NATIONAL LABORATORY on 10/9/2025 3:04:28 PM.
Soft Matter Accepted Manuscript

View Article Online
DOI: 10.1039/D5SM00654F

Published on 30 September 2025. Downloaded by OAKRIDGE NATIONAL LABORATORY on 10/9/2025 3:04:28 PM.

Data Availability Statement

Authors:
Benjamin C. Druecke, Alireza Hooshanginejad, Ranit Mukherjee, Parham Poureslami, and Sungyon Lee*

*Corresponding author: sungyon@umn.edu

The data supporting this article have been included as part of the ESI.

Soft Matter Accepted Manuscript